Pyrolysis and Oxidation of Anisole near 1000 K

M. Pecullan,* K. Brezinsky,† and I. Glassman

Department of Mechanical and Aerospace Engineering, Princeton University, Princeton, New Jersey 08544

Received: October 17, 1996; In Final Form: February 24, 1997[⊗]

Experiments near 1000 K have revealed the thermal decomposition of anisole to proceed exclusively via homolysis of the $O-CH_3$ bond. The anisole decay was observed to be first order even in the presence of oxygen. The distribution of reaction intermediates was virtually independent of equivalence ratio, $\phi \equiv ([\text{anisole}]/[O_2])/([\text{anisole}]/[O_2])_{\text{stoichiometric}}$. Phenol, cresols, methylcyclopentadiene, and CO were major products. Minor species included benzene, cyclopentadiene, ethane, and methane. Trace yields of ethene, toluene, and naphthalenes were observed under all conditions; trace C_2-C_4 species including acetylene, allene, and 1,3-butadiene were observed only in the oxidation experiments. Oxidation occurs preferentially through methylcyclopentadiene. A multichannel reaction scheme is proposed involving the formation of a chemically activated adduct from phenoxy and methyl. The complex reacts to form primarily cresols and methylcyclopentadiene + CO either directly or subsequent to stabilization. A kinetic model for anisole pyrolysis has been developed to predict the disappearance of anisole and the production of reaction intermediates. Excellent agreement is obtained between experimental data and model predictions of anisole, CO, methylcyclopentadiene, and total phenolics.

Introduction

Aromatic hydrocarbons are exploited as a means of boosting octane rating of primarily aliphatic, conventional automotive fuel blends. But the exceptional chemical stability which lends these species their desirable knock properties also implicates them as a source of unburned hydrocarbon emissions. Despite their propensity to soot, aromatics make up a substantial fraction of today's standard unleaded gasoline. In 1990, the industry average gasoline contained 34 vol % aromatics, including 1.7 vol % benzene.[1] Aside from the fuel's initial content, aromatics may also be *formed* in the combustion process from aliphatic molecules (e.g., acetylenes)[2,3] via molecular weight growth mechanisms. Consequently, aromatics have been found to constitute a significant portion of the organic fraction of automobile exhaust.[4] And, benzene emissions are found to be a function of both fuel benzene levels and total hydrocarbon emissions.[1] Kinetic modeling of the high-temperature oxidation of aromatics is a systematic approach to elucidating the chemistry responsible for undesirable tailpipe emissions. The ability to predict—with the goal, ultimately, to control—the chemistry of aromatics is an essential task in the evolution of cleaner practical fuels and combustion systems.

The high-temperature oxidation of benzene, the simplest of all aromatics and a typical fuel component, has been modeled repeatedly[5−8] with consensus regarding the importance (as initially proposed in this laboratory[9]) of the early reaction intermediate phenoxy. Following initiation, phenoxy is formed via reactions of phenyl with O_2 and associated radicals.[10] Emdee et al.[6] modeled the oxidation of benzene at temperatures near 1100 K and concluded that the benzene decay profile was most sensitive to three reactions:

$$H + O_2 \rightarrow O + OH$$

$$C_6H_5O \rightarrow C_5H_5 + CO$$

$$C_6H_5O + H \rightarrow C_6H_5OH$$

The H + O_2 chain branching reaction is essential to the development of the H_2/O_2 radical pool, and almost any high-temperature oxidation system will be sensitive to its rate. The second two reactions determine the fate of the phenoxy radical. As noted by Emdee, the benzene fuel molecule must pass through phenoxy to reach final products, and thus the fate of this radical is very important. The phenoxy radical will also play a key role in the combustion of higher aromatic species, e.g., toluene, whose high-temperature chemistry proceeds through side-chain consumption followed by aromatic ring attack.[6]

The formation and destruction of phenoxy is the dominant route by which the aromatic ring is converted to aliphatic fragments regardless of the identity of the original aromatic molecule. Consequently, phenoxy, in particular its unimolecular decomposition to cyclopentadienyl radical and CO, has been the subject of numerous investigations in the study of combustion chemistry.[11−14] But despite the insight gained from such studies, kinetic modeling of benzene flames has been plagued by gross overprediction of phenoxy concentration.[5,7,8]

As a resonance-stabilized radical, phenoxy may be expected to undergo recombination reactions which compete with its decomposition, particularly in a flame's preheat zone where intermediate temperatures (≈900−1200 K) are encountered. In a practical engine where the fuel is a blend of aromatic and aliphatic constituents, phenoxy−alkyl recombinations may well influence the early flame chemistry and thus the nature of emissions. Indeed, the composition of flame product gases is determined not only by the temperature at the flame front, i.e., the "flame temperature", but also by the time/temperature history of the reactants. In the current study, anisole is exploited as a

† Current address: Department of Chemical Engineering (M/C 110), University of Illinois at Chicago, Chicago, IL 60607.

* To whom correspondence should be addressed.

⊗ Abstract published in *Advance ACS Abstracts,* April 1, 1997.

S1089-5639(96)03203-3 CCC: $14.00

source of phenoxy. At the temperatures employed, anisole decomposes readily to phenoxy and methyl radicals. The anisole oxidation system—at once a mixture of phenoxy, aliphatic fragments, O_2, and, potentially, oxidizing radicals—has been investigated toward development of a comprehensive understanding of the combustion of practical hydrocarbon fuels.

The thermal decomposition of anisole has been investigated in varying degrees of detail by an assortment of experimental techniques. The focus of the earliest gas-phase studies[15,16] was determination of the rate constant for O−methyl bond homolysis:

$$C_6H_5OCH_3 \rightarrow C_6H_5O + CH_3 \quad (1)$$

Over the temperature range 720−795 K, reaction 1 was observed to be the principal course of anisole decay.

Lin and Lin[12] decomposed anisole in a shock tube over the temperature range 1000−1580 K (0.4−0.9 atm). Here anisole was exploited as a source of phenoxy radical in order to determine a rate constant for the unimolecular decomposition of phenoxy to CO and cyclopentadienyl radical (reaction 2). CO production was monitored by resonance absorption spectroscopy and was modeled initially on the basis of the two-step mechanism

$$C_6H_5OCH_3 \rightarrow C_6H_5O + CH_3 \quad (1)$$

$$C_6H_5O \rightarrow C_5H_5 + CO \quad (2)$$

Implicit in this approach is the assumption that the system is free from any additional reactions which may consume phenoxy, thereby reducing the final concentration of CO. But at the longer residence times, CO concentration was found to plateau at a value less than the initial concentration of anisole; even at 1311 K $[CO]_{t=\infty}/[C_6H_5OCH_3]_0$ was less than unity, ≈0.75. It was presumed that the occurrence of reaction 3

$$CH_3 + C_6H_5O \rightarrow o\text{- and } p\text{-}CH_3C_6H_4OH \quad (3)$$

was responsible for the deficiency in the oxygen mass balance. With the inclusion of reaction 4

$$CH_3 + CH_3 \rightarrow C_2H_6 \quad (4)$$

k_3 was modeled to fit the data; i.e., for each set of [CO] data k_3 was varied to account for the "missing" oxygen. At the same time, k_2 was adjusted to maintain agreement with the experimental CO profile. Though Lin and Lin were able to model their data, scatter was evident in the required values of k_3 which ranged from 1×10^{11} to 10×10^{11} cm^3 mol^{-1} s^{-1}.

Mackie and co-workers[17] noted that to establish the validity of Lin and Lin's measurement of k_2 it is important to determine the extent to which reaction 3 influences the phenoxy kinetics. To determine the distribution of oxygen in the products, Mackie studied the thermal decomposition of anisole in a perfectly stirred reactor (850−1000 K, (16−120) × 10^{-3} atm). Methane, ethane, methylcyclopentadiene, and benzene were among the non-oxygenated species detected. The majority of product oxygen was found to exist in cresols and phenol, rather than in CO. The validity of Lin and Lin's work was ultimately neither confirmed nor refuted since the observed yields of phenol could not be accounted for by homogeneous gas-phase abstraction reactions. Nevertheless, the kinetics of anisole decomposition proved to be more complex than is suggested by the four-step mechanism discussed above.

Finally, Arends and co-workers[18] produced a detailed model for the thermolysis of anisole in hydrogen at atmospheric pressure over the temperature range 793−1020 K. Again, the production of phenol could not be modeled strictly via homogeneous gas-phase reactions with physically meaningful rate constants.

TABLE 1: Experimental Conditions

equivalence ratio, ϕ	temp (K)	residence time (ms)	fuel loading (ppm)
pyrolysis	1003	98	1077
1.05	1001	98	1079
0.62	1001	103	1094
1.71	999	100	1090

Notably, no previous anisole oxidation studies have been reported. To further our understanding of the chemistry relevant to practical combustion systems, typically oxidation systems, an investigation of both the pyrolysis and oxidation of anisole was undertaken in this laboratory.

Experimental Technique

Reactor. Anisole pyrolysis and oxidation experiments (Table 1) were carried out in the Princeton atmospheric pressure flow reactor. The design and validation of this apparatus have been detailed repeatedly,[19−21] therefore the following account will be limited to a brief description of reactor operation.

The reactor is an adiabatic, continuous flow device (4 in. i.d.) consisting of an Inconel inlet section joined to a quartz test section. Electric resistance heaters and insulation maintain the walls of the two sections at a chosen reaction temperature. Upstream of the inlet section, a nitrogen carrier gas is heated to reaction temperature by passing through an arc heater a small fraction which is then mixed with the remaining nitrogen. In all, the carrier constitutes approximately 98% of the total molar flow. The reacting mixture is then sufficiently dilute as to absorb any heat released in the reaction process while maintaining near isothermicity. Downstream, oxygen is injected and mixes rapidly such that radial uniformity is achieved prior to fuel injection. The vaporized fuel is injected at the throat of a converging−diverging nozzle which joins the inlet and test sections. Again, mixing is fast (by comparison with convection) and is completed prior to the first sampling point.

The reacting flow is sampled at 15 locations along the center line of the test section, each corresponding to a distinct axial distance from fuel injection which can be equated through the flow velocity to a reaction time. Samples are quenched upon extraction by a water-cooled, stainless steel probe and preserved in a heated multiposition valve (MPV) storage system for subsequent analysis by gas chromatography. The local reaction temperature is measured at the probe tip by a type B thermocouple, silica-coated to block catalysis by bare platinum. Oxygen, CO, and CO_2 are monitored on-line by a Siemens Ultramat 22/O_2 gas analyzer with three independent measurement devices, an electrochemical cell for oxygen and NDIR absorption cells for CO and CO_2. The on-line measurements of CO and CO_2 serve to guide the placement of the reaction in the test section. For a given temperature and equivalence ratio, selection of the flow rate is governed in part by the requirement to capture within the reactor the fuel decay and production of reaction intermediates without conversion of CO to CO_2 and the accompanying heat release.

Analytical Technique. Captured gas samples were analyzed on a Hewlett-Packard Model 5890 gas chromatograph fitted with two capillary columns, each with its own flame-ionization detector (FID), and an SGE column switching unit. The gas sample is injected onto a DB-5 column (J&W Scientific, 30 m, 0.32 mm i.d., 0.25 μm film). C_4 and smaller species are eluted quickly from the DB-5 onto a PORAPlot-Q column (Chrompack, 25 m, 0.32 mm i.d., 10 μm film) where they are separated. A nickel catalyst methanizer upstream of the PORAPlot-Q detector

permits FID detection of CO and CO_2. Prior to elution of any larger species from the DB-5, the column switcher is activated. Species subsequently eluted from the DB-5 are routed to the DB-5 detector, bypassing the PORAPlot-Q. This configuration made possible the separation and quantification, from a single sample, of carbon-containing reaction intermediates over a wide range (C_1-C_{10}) of molecular weights. GC peaks were assigned to species by several techniques including GC-MS, GC-FTIR, and retention time matching to known standards. FID signals were converted to species mole fractions via calibration of the detectors to pure standards for each of the identified species or, in the case of trace species, by carbon number correlations.[22]

The largest uncertainty in the reported yields of reaction intermediates is expected to be that associated with GC calibration. Calibration factors for C_4 and smaller hydrocarbons, CO, CO_2, and benzene were determined by analysis of a custom calibration gas containing these species in known concentrations. Prior to the analysis of each set of 15 samples taken from the flow reactor, this gas mixture was reanalyzed to confirm the calibrations of its constituents. The uncertainty in measurements of these species is estimated to be ±5%. Calibration factors for the cyclopentadienes and aromatics other than benzene were determined via comparison of their FID responses to that of an internal standard (i.e., benzene, whose FID response was well-characterized). For a given species, a solution was prepared of solvent ethanol and small, measured masses of the species in question and benzene. The unknown calibration factor could be correlated to that of benzene by the known component masses in solution, molecular weights, and relative FID responses measured by liquid injection. Measurements of species whose calibrations were determined in this way are estimated to be accurate to within ±10%.

GC analysis of anisole reaction intermediates was complicated by the presence of copious amounts of phenolic species. At the longer reactor residence times, 60−70% of the initial fuel had been converted to phenol and cresols. Strongly polar phenolic compounds readily bond to active sites on quartz surfaces.[23] The GC's quartz injector port liner was found to retain these species, shedding them during subsequent sample injections. For a set of 15 samples analyzed consecutively, the result was a gradual growth in the total carbon count with a 50% carbon deficiency in the first sample and a 50% excess of carbon in the fifteenth. This situation was remedied by deactivating the port liner prior to each experiment by rinsing it in Sylon CT (Supelco, 5% dimethyldisiloxane in toluene). With the implementation of this procedure a carbon balance of unity was readily achieved; i.e., within the uncertainties discussed, the total carbon contained in measured species was equal to the carbon supplied in the initial fuel.

Chemicals. Anisole and all calibration standards were obtained from Aldrich. Anisole purity, specified as 99%, was confirmed by GC analysis. Calibration standards, with the exception of the cyclopentadienes, were quoted ≥99% pure. Methylcyclopentadiene and cyclopentadiene were derived from their dimers which were specified as 93 and 95% pure, respectively.

Results

Comparison of Pyrolysis and Oxidation Data. Indeed for anisole pyrolysis, destruction of the initial fuel was found to proceed almost entirely through cleavage of the weak (64 kcal) phenoxy−methyl bond. In an inert[11,12,17] or hydrogen[18] atmosphere, this unimolecular decomposition had been well-established as the dominant anisole consumption pathway. A comparison of the present pyrolysis data with first-order profiles derived from reported rate constants is given in Figure 1. The

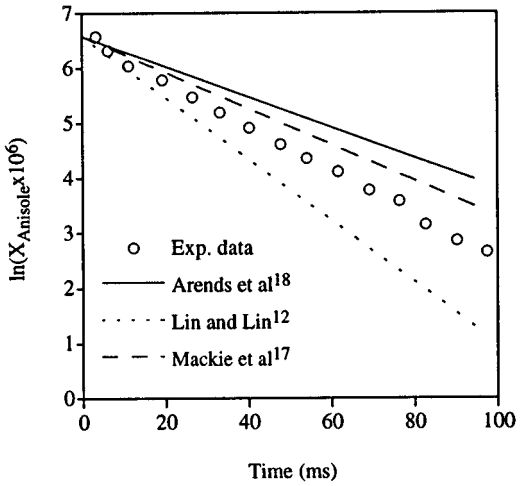

Figure 1. Comparison of experimental pyrolysis data with first-order anisole decay profiles derived from reported rate constants evaluated at 1003 K. X = mole fraction.

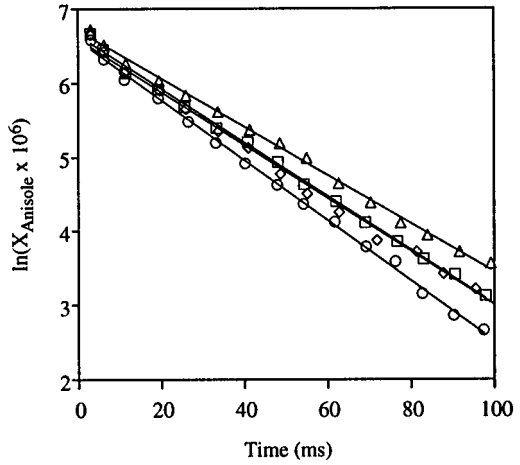

Figure 2. First-order decay profiles for pyrolysis and oxidation of anisole: circle, pyrolysis; square, $\phi = 1.05$; diamond, $\phi = 0.62$; triangle, $\phi = 1.71$. Lines are linear curve fits to experimental data.

data fall within the range of predicted values, and in agreement with earlier work, the observed decay is first-order in anisole.

Interestingly, the current study revealed that even in the presence of oxygen anisole undergoes a first-order decay as verified by the results shown in Figure 2. Here the natural log of anisole mole fraction is demonstrated to be linear with respect to time for oxidation experiments over a range of equivalence ratios. For a plot of this type, deviation from linearity is indicative of second-order kinetic effects. Figure 2 suggests that even for the leanest condition employed, the decay of anisole is still thermally driven. The small differences in slope among the linear curve fits are attributable to the slight variation in temperature among the four experiments with a steeper slope corresponding to a greater temperature and thus a faster rate of decay. Figures 3−6 illustrate the influence of oxygen on the production and consumption of some important reaction intermediates.

As shown in Figure 3, yields of phenol and cresols, major products, are independent of equivalence ratio. Cresol is evolved via a methylcyclohexadienone intermediate formed by addition of methyl to phenoxy at the *ortho* or *para* position.[24] The mechanism, represented globally by reaction 3, is elucidated by consideration of the phenoxy radical as a hybrid of three resonance structures:

The unpaired electron is associated primarily with the ring[17] as depicted by structures **ii** and **iii**. Addition of methyl to a ring site gives *o*- or *p*-methylcyclohexadienone, the keto tautomers

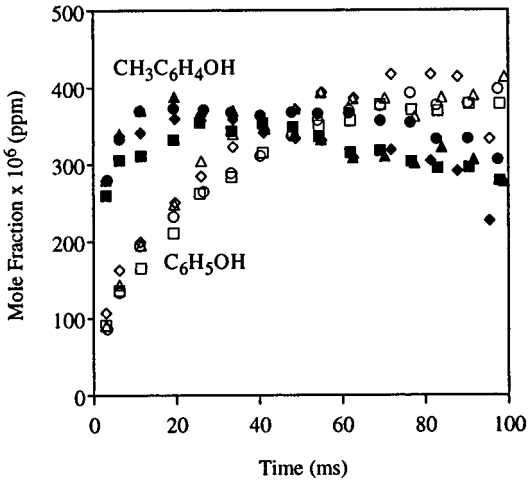

Figure 3. Reaction intermediates observed in the pyrolysis and oxidation of anisole near 1000 K, phenol, and cresols: circle, pyrolysis; square, $\phi = 1.05$; diamond, $\phi = 0.62$; triangle, $\phi = 1.71$.

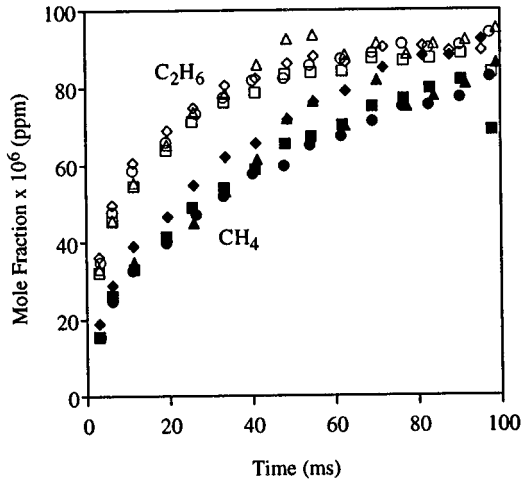

Figure 4. Reaction intermediates observed in the pyrolysis and oxidation of anisole near 1000 K, methane, and ethane: circle, pyrolysis; square, $\phi = 1.05$; diamond, $\phi = 0.62$; triangle, $\phi = 1.71$.

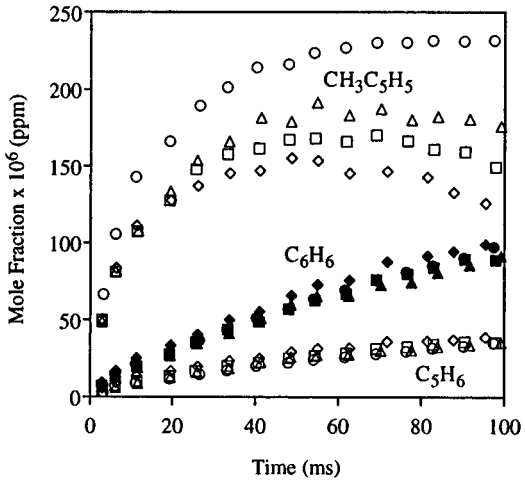

Figure 5. Reaction intermediates observed in the pyrolysis and oxidation of anisole near 1000 K, cyclopentadienes, and benzene: circle, pyrolysis; square, $\phi = 1.05$; diamond, $\phi = 0.62$; triangle, $\phi = 1.71$.

of *o*- and *p*-cresol. Tautomeric equilibrium favors enolization[25] to yield the observed *o*- and *p*-cresols. The recombination of methyl with phenoxy at the O atom (i.e., back-formation of anisole) is not expected to be a significant reaction path as the spin density distribution in the phenoxy radical is just 9% on oxygen.[18]

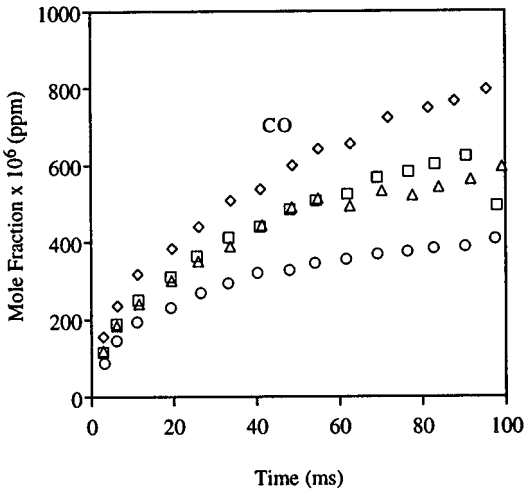

Figure 6. Carbon monoxide observed in the pyrolysis and oxidation of anisole near 1000 K: circle, pyrolysis; square, $\phi = 1.05$; diamond, $\phi = 0.62$; triangle, $\phi = 1.71$.

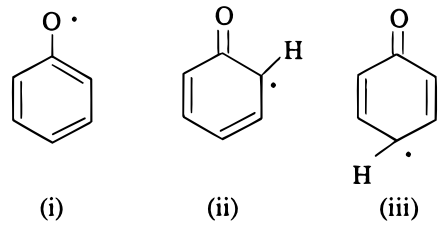

Following an initial period of rapid growth, i.e., $0 < t < 15$ ms, cresol yield is found to reach a pseudo-steady-state which persists until ≈70 ms when a slow decay commences. Phenol undergoes a more gradual growth with yields ultimately exceeding those of the cresols. A similar observation was made by Mackie and co-workers.[17] In their investigation, runs at fixed temperature and pressure showed that phenol yields increased with increasing residence time while cresol yields decreased. It is reasonable to assume that phenol is formed via reaction of phenoxy with a hydrogen donor. But in Mackie's study, some percentage of the total observed phenol (from 54% at 860 K to 98% at 984 K) could not be accounted for by abstraction reactions. It was suggested that cresols were, at least in part, precursors to phenol. In fact, the only mechanism that was found to account for the "excess" phenol was a first-order decomposition of cresol to form phenol directly. An Arrhenius fit to the data yielded the rate constant $k_{fit} = 10^{8.8\pm0.5}$ exp(−35 ± 2 kcal mol^{-1}/*RT*) s^{-1}. As noted by the authors, these empirically determined Arrhenius parameters are not suggestive of a homogeneous gas-phase reaction; at 900 K their estimated rate constant for the $C_6H_5O-CH_3$ bond homolysis is between 2 and 3 orders of magnitude slower than k_{fit}. Furthermore, supporting cresol pyrolysis experiments indicated that decomposition was significant only at temperatures above 1100 K. At 1000 K, the temperature employed in the current study, decomposition of cresol cannot be expected to be a significant source of phenol. For now it is assumed that phenol is derived from the phenoxy radical and a hydrogen donor although, as will be discussed later, the origin of the necessary H atoms is unclear.

Other ϕ-independent products include methane and ethane (Figure 4) derived from methyl radical(s) and cyclopentadiene (Figure 5) evolved from the unimolecular decomposition of phenoxy to CO and cyclopentadienyl radical. Trace yields of ethylene are detected, indicative of ethane consumption. Trace naphthalenes are observed, derived presumably from cyclopentadienyl radicals though the precise mechanism is not conclu-

sively established.[26,27] Benzene yield (Figure 5) is also independent of equivalence ratio.

Oxygen does effect an alteration of the anisole chemistry as evidenced by the methylcyclopentadiene profiles shown in Figure 5. Several mechanisms for $CH_3C_5H_5$ formation may be considered, the most obvious of which is the recombination of C_5H_5 and CH_3 radicals. Alternatively, the cresol radical methylphenoxy may eliminate CO, analogously to phenoxy, to yield methylcyclopentadienyl radical:

$$CH_3C_6H_4O \rightarrow CH_3C_5H_4 + CO \qquad (5)$$

$CH_3C_5H_4$ may then recombine with H but is more likely to form benzene as discussed below. A third reaction pathway is proposed whereby methylcyclopentadiene is formed directly from methyl and phenoxy. This mechanism, to be detailed in the following section, is the dominant mode of methylcyclopentadiene production. For now, it is represented globally by

$$C_6H_5O + CH_3 \rightarrow CH_3C_5H_5 + CO \qquad (6)$$

The methylcyclopentadiene yield was found to depend inversely on initial oxygen concentration. The apparent insensitivity of other reaction intermediate yields to ϕ suggests that methylcyclopentadiene is oxidized preferentially. A comparison of the relative C−H bond strengths among reaction intermediates supports this postulate. The most weakly bonded hydrogen in the system will be most susceptible to attack by molecular oxygen. The cyclopentadienes possess the most readily abstractable hydrogens, i.e., allylic (C−H bond energy $\approx$ 74 kcal[6]). Still, the cyclopentadiene yield is independent of equivalence ratio. Presumably, the C_5H_6 concentration is insufficient to drive its reaction with oxygen. In contrast, the consumption of methylcyclopentadiene, a major product, exhibits a distinct dependence on ϕ with observed yields dwindling with increasing oxygen concentration. Presumably, the oxidation of methylcyclopentadiene will proceed through some ring-opening mechanism to aliphatic fragments and CO. As indicated in Figure 6, an increasing extent of methylcyclopentadiene oxidation is accompanied by the expected growth in CO production. C_2−C_4 oxidation products (e.g., acetylene, ethene, allene, and 1,3-butadiene) are also observed in increasing concentration with decreasing equivalence ratio. Some CO_2 is observed in the oxidation experiments, but yields are not a function of equivalence ratio. The exponential growth of CO_2, indicative of rapid CO to CO_2 conversion, did not occur on the time scale of these experiments.

In the absence of oxygen, methylcyclopentadiene is likely to be consumed via abstraction of H by methyl or phenoxy. Alternatively, it may decompose unimolecularly to $CH_3C_5H_4$ + H. The fate of the methylcyclopentadienyl radical is to form benzene. The radical rearranges to a cyclohexadienyl intermediate which rapidly loses an H atom yielding benzene:[28,29]

$$CH_3C_5H_4 \rightarrow C_6H_7 \rightarrow C_6H_6 + H \qquad (7)$$

As shown in Figure 5, benzene is indeed observed in the pyrolysis of anisole. It follows that the oxidation of methylcyclopentadiene, initiated via H abstraction by molecular oxygen, should effect an increase in the production of benzene. Figure 5 illustrates that this supposition is not upheld by the experimental data; $CH_3C_5H_5$ oxidation is not accompanied by a benzene yield in excess of that which is attributable to pyrolytic chemistry. This result suggests the existence of a rapid oxidation pathway whereby the $CH_3C_5H_4$ radical precursor to benzene is consumed at a rate that is competitive with reaction 7. Alternatively, methylcyclopentadiene conversion may proceed by radical addition to the parent and subsequent decomposition (i.e., $CH_3C_5H_4$ production is averted entirely). By either mechanism methylcyclopentadiene could be oxidized, without a concomitant increase in benzene, to CO and the C_2−C_4 species mentioned above.

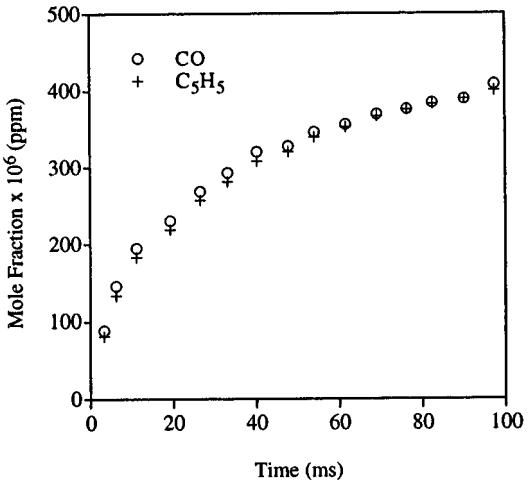

Figure 7. Comparison of CO and sum of C_5H_5 moieties observed in the pyrolysis of anisole at 1003 K. $C_5H_5 = C_5H_6 + CH_3C_5H_5 + C_6H_6 + C_6H_5CH_3 + 2(C_{10}H_8 + C_{10}H_{10})$.

Validation of Pyrolysis Chemistry. In the absence of oxidative chemistry, the mechanistic interpretation put forth implies a balance of CO and the sum of C_5H_5 moieties. As discussed, CO is produced proportionately with the cyclopentadienes. The sum of C_5H_5 moieties must include not just the cyclopentadienes themselves, but any species that are derived from secondary reactions of C_5H_6 and $CH_3C_5H_5$ or their respective radicals. These species include benzene, naphthalenes, and toluene. Benzene is derived from the methylcyclopentadienyl radical, and trace yields of toluene are presumed to be derived from benzene. Naphthalenes (i.e., naphthalene and dihydronaphthalene) are evolved via recombination of two cyclopentadienyl radicals and are therefore counted twice in the C_5H_5 tally. The anisole pyrolysis data in Figure 7 confirm the proposed agreement between CO yield and the sum yield of C_5H_5 derivatives. This result supports, qualitatively, the proposed chemistry. In order to assess the relative importance of the various phenoxy reaction pathways and to gain a more quantitative understanding of the kinetics following the initial O−CH_3 bond homolysis, detailed reaction modeling has been employed.

Kinetic Modeling

At the experimental conditions employed in this study the reaction intermediate yields are, with a few exceptions, insensitive to equivalence ratio. It can be inferred that, even in the presence of oxygen, the chemistry is primarily pyrolytic. Therefore, accurate characterization of the pyrolysis chemistry is essential to the development of a model for the oxidation of anisole.

Model Description. A model for the pyrolysis of anisole (Table 2) consisting of 66 reversible reactions involving 31 species has been developed. The reacting flow was treated numerically as a homogeneous, zero-dimensional, adiabatic, constant-pressure system using CHEMKIN.[30] Elementary reaction rate parameters for which measured values do not exist were obtained from thermodynamic estimations, QRRK analysis, or semiempirical molecular orbital calculations or by comparison with analogous reactions. Thermodynamic properties (Table 3) were taken from the CHEMKIN thermodynamic data base,[31] Burcat,[32] and Ritter[29] or in many cases were estimated by group additivity methods using THERM.[33,34]

TABLE 2: Reaction Mechanism[a]

reaction	*A*	*n*	E_a	ref
$C_6H_5OCH_3 \rightarrow C_6H_5O + CH_3$	3.00E+15	0.00	63000	*b*
$C_6H_5OCH_3 + CH_3 \rightarrow C_6H_5OCH_2 + CH_4$	5.01E+11	0.00	10500	18
$C_6H_5OCH_3 + C_6H_5O \rightarrow C_6H_5OCH_2 + C_6H_5OH$	4.17E+11	0.00	16060	18
$C_6H_5OCH_2 \rightarrow C_6H_5CHO + H$	3.16E+12	0.00	21500	18
$C_6H_5O + CH_3 \rightarrow (H)(CH_3)C_6H_4O$ *	2.28E+86	−21.60	36090	*c*
$C_6H_5O + CH_3 \rightarrow 5\text{-}CH_3C_5H_5 + CO$ *	2.05E+75	−18.30	38880	*c*
$C_6H_5O + CH_3 \rightarrow CH_3C_6H_4O + H$ *	3.33E+39	−7.80	31670	*c*
$C_6H_5O + CH_3 \rightarrow CH_3C_6H_4OH$ *	2.31E+73	−17.40	38780	*c*
$C_6H_5O + CH_3 \rightarrow C_6H_4OH + CH_3$ *	1.29E−31	13.20	15580	*c*
$(H)(CH_3)C_6H_4O \rightarrow CH_3C_6H_4OH$ *	2.73E+60	−13.70	64300	*c*
$(H)(CH_3)C_6H_4O \rightarrow 5\text{-}CH_3C_5H_5 + CO$ *	1.18E+47	−10.30	51910	*c*
$C_6H_5O \rightarrow CO + C_5H_5$	7.40E+11	0.00	43853	14
$C_6H_5O + H \rightarrow C_6H_5OH$	2.50E+14	0.00	0	41
$C_6H_5OH + H \rightarrow C_6H_6 + OH$	2.21E+13	0.00	7930	41
$C_6H_5OH + CH_3 \rightarrow C_6H_5O + CH_4$	2.51E+11	0.00	8000	24
$C_6H_5O + C_2H_6 \rightarrow C_6H_5OH + C_2H_5$	3.02E+11	0.00	11500	*d*
$C_6H_5OH + H \rightarrow C_6H_5O + H_2$	1.15E+14	0.00	12400	41
$5\text{-}CH_3C_5H_5 \rightarrow 1\text{-}CH_3C_5H_5$	7.57E+12	0.00	35100	*c*
$1\text{-}CH_3C_5H_5 \rightarrow 2\text{-}CH_3C_5H_5$	2.56E+14	0.00	55700	*c*
$1\text{-}CH_3C_5H_5 + H \rightarrow CH_3C_5H_4 + H_2$	2.19E+08	1.77	3000	*e*
$2\text{-}CH_3C_5H_5 + H \rightarrow CH_3C_5H_4 + H_2$	2.19E+08	1.77	3000	*e*
$5\text{-}CH_3C_5H_5 + H \rightarrow CH_3C_5H_4 + H_2$	1.08E+08	1.77	3000	*f*
$CH_3C_5H_4 + H \rightarrow 1\text{-}CH_3C_5H_5$	1.00E+14	0.00	0	*g*
$CH_3C_5H_4 + H \rightarrow 2\text{-}CH_3C_5H_5$	1.00E+14	0.00	0	*g*
$CH_3C_5H_4 + H \rightarrow 5\text{-}CH_3C_5H_5$	1.00E+14	0.00	0	*g*
$5\text{-}CH_3C_5H_5 \rightarrow CH_3 + C_5H_5$	1.00E+16	0.00	67500	29
$CH_3C_5H_4 + H \rightarrow C_5H_5 + CH_3$	8.00E+13	0.00	0	29
$1\text{-}CH_3C_5H_5 + CH_3 \rightarrow CH_3C_5H_4 + CH_4$	3.11E+11	0.00	5500	*e*
$2\text{-}CH_3C_5H_5 + CH_3 \rightarrow CH_3C_5H_4 + CH_4$	3.11E+11	0.00	5500	*e*
$5\text{-}CH_3C_5H_5 + CH_3 \rightarrow CH_4 + CH_3C_5H_4$	1.56E+11	0.00	5500	*f*
$1\text{-}CH_3C_5H_5 + C_6H_5O \rightarrow CH_3C_5H_4 + C_6H_5OH$	3.16E+11	0.00	8000	*e*
$2\text{-}CH_3C_5H_5 + C_6H_5O \rightarrow CH_3C_5H_4 + C_6H_5OH$	3.16E+11	0.00	8000	*e*
$5\text{-}CH_3C_5H_5 + C_6H_5O \rightarrow CH_3C_5H_4 + C_6H_5OH$	1.58E+11	0.00	8000	*f*
$1\text{-}CH_3C_5H_5 + C_5H_5 \rightarrow CH_3C_5H_4 + C_5H_6$	3.16E+11	0.00	8000	*h*
$2\text{-}CH_3C_5H_5 + C_5H_5 \rightarrow CH_3C_5H_4 + C_5H_6$	3.16E+11	0.00	8000	*h*
$5\text{-}CH_3C_5H_5 + C_5H_5 \rightarrow CH_3C_5H_4 + C_5H_6$	1.58E+11	0.00	8000	*h*
$H + C_6H_6 \rightarrow CH_3C_5H_4$	5.22E+28	−4.30	28800	29
$H + C_6H_6 \rightarrow c\text{-}C_6H_7$	8.18E+57	−13.20	26300	29
$c\text{-}C_6H_7 \rightarrow CH_3C_5H_4$	5.00E+12	0.00	38100	29
$CH_2C_6H_4OH + H \rightarrow CH_3C_6H_4OH$	1.80E+14	0.00	0	18
$CH_3C_6H_4OH + CH_3 \rightarrow CH_3C_6H_4O + CH_4$	2.51E+11	0.00	8000	*i*
$CH_3C_6H_4OH + C_6H_5O \rightarrow CH_3C_6H_4O + C_6H_5OH$	1.05E+11	0.00	9500	*j*
$C_6H_5OH + CH_2C_6H_4OH \rightarrow C_6H_5O + CH_3C_6H_4OH$	1.05E+11	0.00	9500	*j*
$CH_3C_6H_4OH + CH_3 \rightarrow CH_2C_6H_4OH + CH_4$	3.16E+11	0.00	9500	*k*
$CH_3C_6H_4OH + H \rightarrow CH_3C_6H_4O + H_2$	1.15E+14	0.00	12400	*i*
$CH_3C_6H_4O + H \rightarrow CH_3C_6H_4OH$	2.50E+14	0.00	0	*l*
$CH_3C_6H_4O \rightarrow CO + CH_3C_5H_4$	7.40E+11	0.00	43853	*l*
$C_5H_5 + C_5H_5 \rightarrow C_{10}H_8 + H_2$	1.00E+11	0.00	0	18
$C_5H_6 + CH_3 \rightarrow CH_4 + C_5H_5$	3.11E+11	0.00	5500	49
$C_5H_6 + C_2H_5 \rightarrow C_5H_5 + C_2H_6$	4.67E+11	0.00	5500	*m*
$C_5H_5 + H \rightarrow C_5H_6$	1.00E+14	0.00	0	6
$C_5H_6 + H \rightarrow C_5H_5 + H_2$	2.19E+08	1.77	3000	6
$C_5H_6 + C_6H_5O \rightarrow C_5H_5 + C_6H_5OH$	3.16E+11	0.00	8000	6
$C_5H_6 + CH_3C_6H_4O \rightarrow C_5H_5 + CH_3C_6H_4OH$	3.16E+11	0.00	8000	*l*
$C_6H_6 + CH_3 \rightarrow C_6H_5 + CH_4$	2.00E+11	0.00	11233	50
$C_6H_5 + H \rightarrow C_6H_6$	2.20E+14	0.00	0	51
$C_6H_6 + H \rightarrow C_6H_5 + H_2$	2.50E+14	0.00	16000	52
$C_6H_5 + C_6H_5OH \rightarrow C_6H_6 + C_6H_5O$	4.91E+12	0.00	4400	53
$C_6H_5CH_3 \rightarrow C_6H_5 + CH_3$	1.40E+16	0.00	99800	54
$2CH_3\ (+M) \rightarrow C_2H_6\ (+M)$	2.12E+16	−0.97	620	55
low-press. limit:	1.77E+50	−9.67	6220	
Troe centering:	0.532	151	1038	4970
$H + CH_4 \rightarrow CH_3 + H_2$	6.60E+08	1.62	10840	55
$H + CH_3\ (+M) \rightarrow CH_4\ (+M)$	1.27E+16	−0.63	383	55
low-press. limit:	2.48E+33	−4.76	2440	
Troe centering:	0.783	74	2941	6964
$H + C_2H_4\ (+M) \rightarrow C_2H_5\ (+M)$	1.08E+12	0.45	1820	55
low-press. limit:	1.20E+42	−7.62	6970	
Troe centering:	0.975	210	984	4374
$H + C_2H_6 \rightarrow C_2H_5 + H_2$	1.15E+08	1.90	7530	55
$2CH_3 \rightarrow H + C_2H_5$	4.99E+12	0.10	10600	55
$CH_3 + C_2H_6 \rightarrow C_2H_5 + CH_4$	6.14E+06	1.74	10450	55

[a] Units: cm^3, mol, s, cal. In this and all tables $E\pm n \equiv \times 10^{\pm n}$. [b] From the rate constant of Arends,[18] given as $10^{15.3(\pm 0.2)} \exp[(-63.6(\pm 0.7)\ \text{kcal mol}^{-1})/RT]\ s^{-1}$. [c] This work. [d] Estimated from $HO_2 + C_2H_6 \rightarrow H_2O_2 + C_2H_5$.[47] [e] Estimated from analogous abstraction of H from C_5H_6. [f] Estimated from analogous abstraction of H from C_5H_6; *A* factor divided by 2 since $5\text{-}CH_3C_5H_5$ possesses only one easily abstractable H. [g] *A* factor for $C_5H_5 + H$. [h] Rate parameters from $CH_3C_5H_5 + C_6H_5O$. [i] Estimated from analogous abstraction of H from phenol. [j] Estimated from $CH_3C_6H_4OH + C_6H_5CH_2 \rightarrow CH_3C_6H_4O + C_6H_5CH_3$.[6] [k] Estimated from analogous reaction of toluene and methyl.[48] [l] Rate parameters from analogous reaction of phenoxy. [m] Estimated from $C_5H_6 + CH_3 \rightarrow C_5H_5 + CH_4$. [n] Asterisk indicates rate parameters are pressure dependent, calculated for $P = 1$ atm.

TABLE 3: Thermodynamic Properties for Select Species[a]

species	$H_f(298)$	$S(298)$	$C_p(300)$	$C_p(400)$	$C_p(500)$	$C_p(600)$	$C_p(800)$	$C_p(1000)$	$C_p(1500)$	ref
C_5H_5	63.60	66.80	18.43	24.47	29.57	33.63	38.95	42.76	48.06	32
C_5H_6	32.10	65.52	18.13	24.46	30.12	34.82	41.22	45.87	52.36	32
C_6H_5	78.50	68.91	19.00	25.45	30.96	35.52	42.10	46.58	52.76	32
C_6H_6	19.81	64.37	19.92	27.09	33.25	38.38	45.87	51.05	58.31	32
C_6H_5O	9.30	73.63	22.65	29.88	35.80	40.59	47.53	52.22	58.96	32
C_6H_5OH	−23.03	75.33	24.93	32.38	38.63	43.68	50.73	55.56	62.37	32
$C_6H_5OCH_3$	−17.10	84.01	29.67	38.91	46.53	52.77	62.06	68.33	77.22	*b*
$C_6H_5OCH_2$	79.99	88.28	28.35	37.07	43.97	49.42	57.08	62.04	69.80	*b*
$CH_2C_6H_4OH$	7.15	86.21	30.71	40.82	49.33	56.47	67.43	75.11	72.77	*b*
$CH_3C_6H_4OH$	−31.62	85.06	29.97	38.82	46.53	52.93	62.08	68.61	77.64	32
$CH_3C_6H_4O$	2.80	78.89	50.37	52.48	54.65	56.85	61.20	65.29	73.43	32
$(H)(CH_3)C_6H_4O$	−15.02	78.12	28.78	38.42	46.39	52.96	62.76	69.39	78.70	*b*
C_6H_4OH	39.25	77.68	23.52	30.35	35.95	40.51	47.24	51.75	58.15	*b*
5-$CH_3C_5H_5$	28.30	73.01	22.23	29.25	35.56	41.18	50.48	57.46	67.19	29
2-$CH_3C_5H_5$	24.38	74.16	28.07	35.72	41.88	46.85	54.29	59.98	67.74	32
1-$CH_3C_5H_5$	22.81	74.44	24.35	32.19	38.73	44.17	52.44	58.22	66.80	*b*
$CH_3C_5H_4$	48.06	75.37	23.15	29.92	35.94	41.23	49.78	55.93	63.86	29
c-C_6H_7	49.86	72.02	20.88	28.59	35.04	40.43	48.66	54.39	62.67	29

[a] Units: H_f, kcal/mol; S and C_p, cal/(mol K). [b] Estimated using group additivity methods.[33,34]

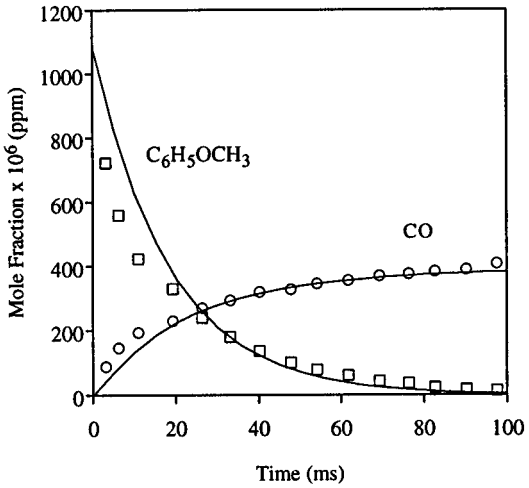

Figure 8. Comparison of experimental pyrolysis data and model prediction of anisole and carbon monoxide. Solid lines indicate model results.

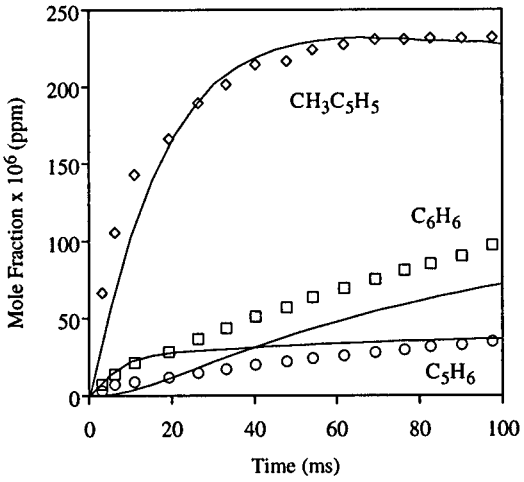

Figure 9. Comparison of experimental pyrolysis data and model prediction of cyclopentadiene, methylcyclopentadiene, and benzene. Solid lines indicate model results.

Model Development and Discussion. Experimental pyrolysis data are compared with model predictions of anisole decay and CO production in Figure 8. Predictions of these species, descriptors of overall reaction progress, match experiment well. The rate constant for the thermal decomposition of anisole was taken from the work of Arends et al.[18] However, the rate parameters were adjusted (within the uncertainty quoted by Arends) to speed the decomposition. While the modeling results suggest that additional optimization may be warranted, the authors chose not to adjust further the Arrhenius parameters in order to avoid excessive "tweaking" of the measured rate constant. Furthermore, the value of k_1 given in Table 2 provides the best match between model predictions and experimental data over the whole 100 ms reaction time. Adjustment of k_1 to better match the data at the early times is at the expense of agreement at the later times.

Close agreement between model and experiment is obtained for methylcyclopentadiene as shown in Figure 9. Predictions of cyclopentadiene and benzene (also Figure 9) are not quite as good. The cyclopentadiene model profile is actually derived from the sum of the parent and its radical. Cyclopentadienyl, a resonantly stabilized radical, may realistically be expected to build to high concentration (relative to other, more reactive radicals) in the flow reactor. The radical is then likely to encounter a source of H in the sampling probe, e.g., condensate on the probe's inner surface, and be detected as the stable species cyclopentadiene. The early, sharp rise in the combined C_5H_5/C_5H_6 model profile is due to rapid growth of the radical concentration. C_5H_5 production is attributed primarily to reaction 2 whose rate parameters have been reported by a number of investigators.[12−14] At 1000 K, these reported rate constants vary by a factor of 3. Frank's[14] value is chosen here. Use of the slower rate constant of Lin[12] does improve the cyclopentadiene prediction, but Frank's value provides the best overall agreement between model and experiment.

Two isomers of methylcyclopentadiene, 1- and 2-$CH_3C_5H_5$, are observed experimentally. The experimental methylcyclopentadiene profiles in Figures 9 and 5 represent the sum yield of both isomers. Likewise, the model profile represents the sum of the predicted yields of 1- and 2-$CH_3C_5H_5$. Interestingly, it is the 5- isomer which is formed initially; the observed 1- and 2-isomers arise via [1,5] sigmatropic rearrangement(s). The importance of these isomerization reactions and the estimation of their rate parameters will be discussed shortly.

Cyclopentadienyl, as mentioned above, and methyl are relatively unreactive radicals, and their lifetimes are expected to be sufficiently long as to facilitate recombination reactions. Attempts to model methylcyclopentadiene production strictly via recombination of these two radicals would not reproduce the observed rapid growth of the species in the first 20 ms. Arends[18] suggested that H attack on methylcyclohexadienone, the keto precursor to cresol, can yield methylcyclopentenyl and CO. Here it is considered that the initially formed methylcyclohexadienone complex may possess sufficient energy (gained

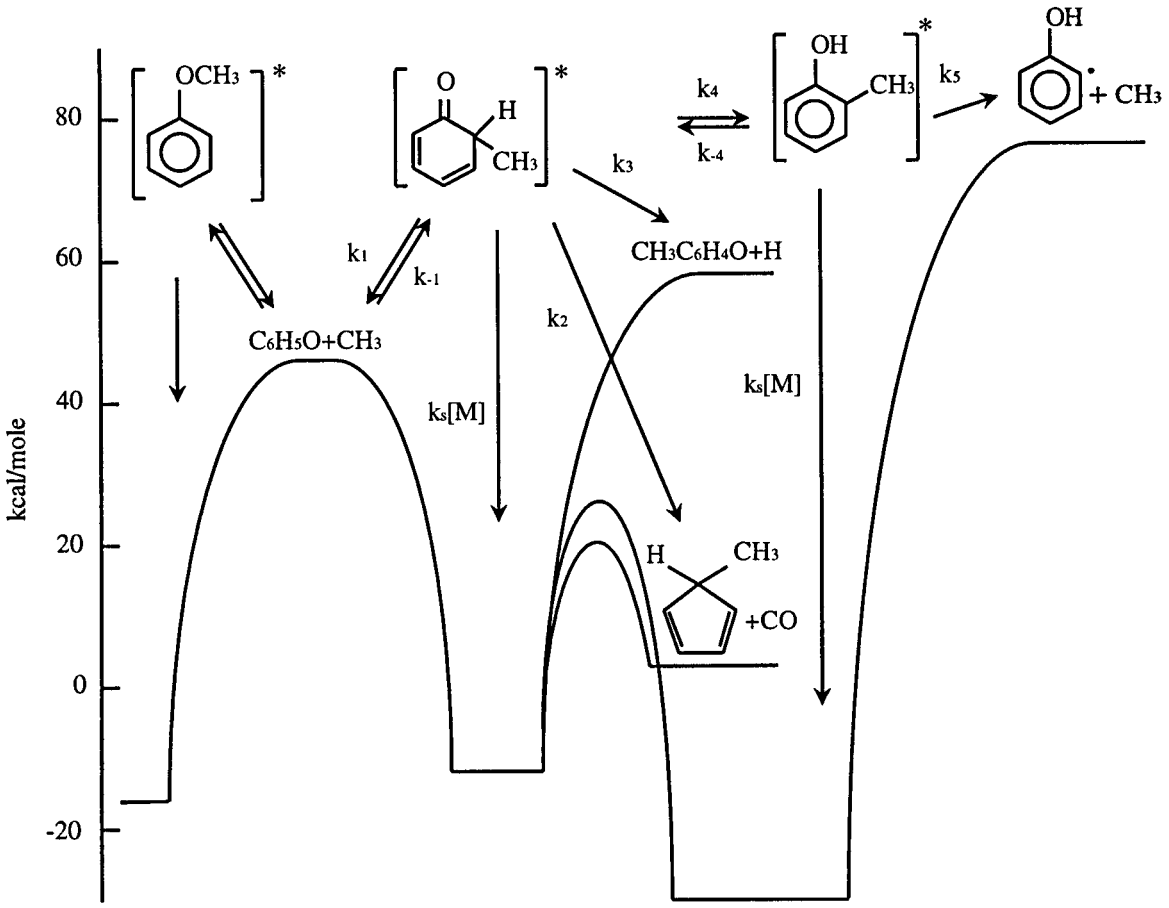

Figure 10. Potential energy diagram for $C_6H_5O + CH_3$.

from creation of the new chemical bond) to decompose to methylcyclopentadiene and CO. This molecular elimination reaction was first proposed by Cypres and Bettens[35] to explain the formation of methylcyclopentadiene in their cresol pyrolysis experiments. The authors postulated the expulsion of CO following an isomerization of cresol to a methylcyclohexadienone intermediate.

The CHEMACT code[36] was used to treat the multichannel reaction scheme initiated by recombination of the phenoxy and methyl radicals. CHEMACT employs the QRRK (quantum Rice−Ramsperger−Kassel) theory of chemical activation to estimate apparent rate constants for the various reaction pathways that proceed through formation of an energized complex by radical recombination. The potential energy diagram in Figure 10 illustrates the treatment of phenoxy−methyl recombination by chemical activation principles. C_6H_5O and CH_3 may form directly three distinct adducts depending upon the recombination site. Recombination at the O atom to form $C_6H_5OCH_3$* is not expected to be a significant reaction path in accordance with the electron density arguments given previously. So discussion is limited to the recombination of CH_3 with C_6H_5O at a ring site to form the chemically activated *o*- and *p*-(H)$(CH_3)C_6H_4O$* adducts.

As proposed above, the methylcyclohexadienone complex may eliminate CO to yield 5-$CH_3C_5H_5$. It is important to consider in addition all reactions that may realistically be expected to occur since calculation of the rate constant for a given channel will be dependent upon the rate constants of other existing channels. Therefore, loss of H to yield the methylphenoxy radical, in effect the displacement of H by methyl, is also considered. Back-reaction of the adduct to the initial radicals represents an additional decomposition pathway. Alternatively, (H)$(CH_3)C_6H_4O$* may be stabilized by collisions or may isomerize to form a second chemically activated molecule, $CH_3C_6H_4OH$*. $CH_3C_6H_4OH$* may in turn decompose to CH_3 and C_6H_4OH or yield cresol by stabilization. It should be noted here that no attempt has been made to distinguish between the *o*- and *p*-isomers of either adduct or the corresponding stabilized species, methylcyclohexadienone and cresol. Implicit in this treatment is the assumption that reactions of these species are not isomer selective. This is consistent with the RRKM treatment of $C_6H_5O-CH_3$ recombination by Lin and Lin.[37] Lin and Lin evaluated the branching ratio for isomerization versus stabilization of the methylcyclohexadienone complex and reported a single value for the energy barrier to isomerization. In the current analysis *ortho* and *para* forms have been treated equivalently, and the modeling results have given no indication that a distinction is necessary.

Inputs to the CHEMACT code are given in Table 4. High-pressure rate constants k_1-k_5, k_{-1}, and k_{-4} were derived from thermodynamic estimations or by comparison with analogous reactions. Thermodynamic consistency has been maintained for the reaction pairs 1 and 4. Calculated apparent rate constants for reaction of C_6H_5O and CH_3 to products are given in Table 5. Comparison of rate expressions evaluated at $T = 1000$ K reveals that channels 3 and 5 are negligible at the experimental conditions. Dissociation to initial reactants of (H)$(CH_3)C_6H_4O$* (no reaction) is found to be significant. However, stabilization of the initially formed complex clearly dominates accounting for 60% of the collisions that create the adduct. Recall that in this context the term "stabilized" refers to *thermal* stabilization; i.e., a stabilized species possesses a Boltzmann distribution of energies. Further reaction of the thermalized species is possible and must be accounted for.

Decomposition of (H)$(CH_3)C_6H_4O$ to the initial reactants is automatically included in the model since the reactions are written reversibly. However, decomposition/isomerization to other products, in particular 5-$CH_3C_5H_5$ + CO and

TABLE 4: CHEMACT Input Parameters for Analysis of $C_6H_5O + CH_3$

k	A^a	E_a (kcal/mol)	source
1	1.04E+14	0.0	*b*
−1	5.66E+17	57.4	*c*
2	7.40E+11	32.5	*d*
3	3.26E+15	67.9	*e*
4	5.67E+13	39.0	*f*
−4	1.75E+12	55.6	*c*
5	1.40E+16	99.8	*g*
$\langle\nu\rangle = 1141$ cm^{-1}			*h*
$\sigma = 5.10$ Å			*i*
$\epsilon/k = 595$ K			*i*

[a] Units: s^{-1} (except $A_1 \sim$ cm^3 mol^{-1} s^{-1}). [b] A_1 set equal to 10 times A factor for $C_6H_5O + CH_3 \rightarrow C_6H_5OCH_3$ according to electron density arguments (see text). [c] Calculated from forward rate parameters on the basis of thermodynamics. [d] A_2 given as A factor for $C_6H_5O \rightarrow C_5H_5 + CO$. $E_{a,2}$ equal to ΔH_R (17 kcal) plus intrinsic activation energy of phenoxy reaction (16 kcal), reduced by 0.5 kcal/mol. [e] A_3 and $E_{a,3}$ calculated from thermodynamics with $A_{-3} = 1.0E+14$. [f] A_4 determined from transition state theory, $A = (ekT/h)\exp(\Delta S^{\ddagger}/R)$. Transition state was assumed to be tight, i.e., $\Delta S^{\ddagger} \approx 0$. $E_{a,4}$ estimated by analogy with tautomerization reaction 2-pyridone $\rightarrow$ 2-hydroxypyridine.[56] [g] $E_{a,5}$ and A_5 by analogy with $C_6H_5CH_3 \rightarrow C_6H_5 + CH_3$.[54] [h] Vibrational frequencies estimated by Lin and Lin[37] on the basis of the spectra of *p*-benzoquinone and toluene. [i] Lennard−Jones parameters estimated by methods detailed in Reid et al.[57]

$CH_3C_6H_4OH$, must be considered as well. The multichannel unimolecular reaction of $(H)(CH_3)C_6H_4O$ was treated using the CHEMACT companion code DISSOC. The relative importance of the direct (prior to stabilization of the adduct) product formation routes with respect to the indirect (following stabilization) routes was determined by flux analysis, discussed below.

Flux analysis is simply the determination of the "flux" or rate (mol cm^{-3} s^{-1}) of each reaction at each time step. A flux diagram (Figure 11) is then a convenient pictorial representation of the flow of reaction intermediates. In Figure 11 each arrow is representative of a given reaction in the indicated direction; the forward and reverse of a reaction are depicted individually. The magnitude of the flux of a reaction is indicated by the weight of its arrow. This analysis was performed for $t = 15$ ms, the residence time corresponding to ≈50% anisole conversion and steep gradients in species profiles. Note that every reaction in Table 2 is not represented in Figure 11. Only the most significant reactions have been included.

Immediately, Figure 11 reveals that at $t = 15$ ms the indirect routes (i.e., via stabilized $(H)(CH_3)C_6H_4O$) are more significant sources of 5-$CH_3C_5H_5$ and $CH_3C_6H_4OH$ than the direct reactions. The flux of cresol through isomerization of the stabilized adduct is, on average over the 100 ms reaction time, roughly 5 times the flux by way of the direct reaction. The flux of methylcyclopentadiene through decomposition of $(H)(CH_3)C_6H_4O$ is on average an order of magnitude greater than the flux from phenoxy and methyl directly. Together, these two reaction pathways account for roughly 90% of the total methylcyclopentadiene formed. Recombination of methyl and cyclopentadienyl radicals accounts for the remainder.

Formation of methylcyclopentadiene through addition of CH_3 to either C_5H_5 or C_6H_5O necessarily yields the 5-isomer. The 1- and 2-forms are derived via sigmatropic rearrangement(s).[38,39] A [1,5] sigmatropic hydrogen shift yields 1-$CH_3C_5H_5$, which may itself undergo a [1,5] shift to yield 2-$CH_3C_5H_5$. Two GC peaks have been identified by MS as isomers of methylcyclopentadiene.[21] On the basis of equilibrium considerations,[39] these peaks are assigned to 1- and 2-$CH_3C_5H_5$. While thermodynamic properties do not differ vastly among isomers, the kinetic stability of the 5-isomer does contrast significantly with that of the 1- and 2-forms. Specifically, at 1000 K 5-$CH_3C_5H_5$ decomposes readily via cleavage of the $C_5H_5-CH_3$ bond ($E_a = 67.5$ kcal). In contrast, the activation energy for analogous decomposition of 1- or 2-$CH_3C_5H_5$, estimated from thermodynamics, is approximately 95 kcal, rendering these reactions negligible. The pyrolysis data in Figure 9 suggest that at the later residence times methylcyclopentadiene persists in a pseudo-steady-state. In order to reproduce the observed stability of methylcyclopentadiene in the anisole pyrolysis system, it is necessary to include $CH_3C_5H_5$ isomerization reactions in the model. Rate parameters for the two isomerization reactions (5- to 1-$CH_3C_5H_5$ and 1- to 2-$CH_3C_5H_5$) are derived from $\Delta H^{\ddagger}$ and $\Delta S^{\ddagger}$, estimated from semiempirical molecular orbital calculations using MOPAC[40] (Table 6). The results are consistent with the observations of McClean and Haynes,[39] who showed that 5-$CH_3C_5H_5$ rearranged "very rapidly" to 1-$CH_3C_5H_5$, which then rearranged "more slowly" to 2-$CH_3C_5H_5$.

Prediction of total phenolics (Figure 12) agrees well with experiment though the split between phenol and cresols demonstrates poor agreement with cresols overpredicted by a factor of 2; at 98 ms total phenolics are comprised of approximately equal parts phenol and cresols while the model predicts essentially only cresols. An accompanying underprediction of methane and ethane (Figure 13) is consistent with this result; methyl groups are trapped in excess cresols, unavailable to reactions forming methane and ethane. All attempts to improve prediction of these species by optimization—within realistic limits—of rate parameters were unsuccessful.

In particular, reactions of phenoxy and methyl radicals with the intermediate *o*- and *p*-methylcyclohexadienones were investigated. These molecules possess a weak, abstractable hydrogen atom and are also polar, so abstraction could be a fast (low E_a) process. Mulcahy and Williams,[24] in their study of methyl radical reactions with phenol, observed larger yields of CH_4 than could be accounted for by abstraction from phenol. They attributed their surplus CH_4 to an unusually rapid reaction between CH_3 and methylcyclohexadienone intermediates. Nevertheless, adoption of large rate constants (as high as 10^{12} cm^3 mol^{-1} s^{-1}) for the reactions

$$C_6H_5O + (H)(CH_3)C_6H_4O \rightarrow C_6H_5OH + CH_3C_6H_4O$$

$$CH_3 + (H)(CH_3)C_6H_4O \rightarrow CH_4 + CH_3C_6H_4O$$

did not reproduce the present experimental phenol and methane profiles. In the present system, $[(H)(CH_3)C_6H_4O]$ is at best 2 orders of magnitude less than $[CH_3]$ or $[C_6H_5O]$, and thus the above reactions cannot compete with reactions of phenoxy and methyl with one another.

As shown in Figure 11, recombination of phenoxy with H is virtually the sole source of phenol in the present model. The rate constant for the reaction (2×10^{14} s^{-1}, He et al.[41]) is large. However, formation of phenol via this recombination is limited by the deficiency of atomic hydrogen in this system.

An attempt was made to model the production of phenol directly from anisole. Arends[18] proposed the addition of H to anisole at the *ortho* or *para* position of the aromatic nucleus followed by methyl elimination to yield (keto)phenol. In the current study a phenol formation pathway not involving atomic hydrogen was sought. Unimolecular elimination of the methylene singlet from anisole was postulated. Insertion of $:CH_2$ into O−H bonds to form methyl ethers is known to occur.[42] In accordance with microreversibility the reverse reaction, expulsion from O−CH_3, must be possible. The reaction

$$C_6H_5OH + :CH_2 \rightarrow C_6H_5OCH_3 \qquad (8)$$

TABLE 5: Apparent Reaction Rate Constants[a,b] Calculated via QRRK Analysis

reaction	A	n	E_a	$k_{1000\ K}$
$(H)(CH_3)C_6H_4O^* \rightarrow C_6H_5O + CH_3$	1.106E+58	−12.27	35190	3.49E+13
$C_6H_5O + CH_3 \rightarrow (H)(CH_3)C_6H_4O$	2.277E+86	−21.56	36090	6.16E+13
$C_6H_5O + CH_3 \rightarrow 5\text{-}CH_3C_5H_5 + CO$	2.049E+75	−18.29	38880	8.78E+11
$C_6H_5O + CH_3 \rightarrow CH_3C_6H_4O + H$	3.331E+39	−7.78	31670	1.82E+09
$C_6H_5O + CH_3 \rightarrow CH_3C_6H_4OH$	2.313E+73	−17.37	38780	6.00E+12
$C_6H_5O + CH_3 \rightarrow C_6H_4OH + CH_3$	1.292E−31	13.20	15580	2.02E+05
$(H)(CH_3)C_6H_4O \rightarrow 5\text{-}CH_3C_5H_5 + CO$	1.180E+47	−10.32	51910	6.70E+04
$(H)(CH_3)C_6H_4O \rightarrow CH_3C_6H_4OH$	2.732E+60	−13.73	64300	1.92E+05

[a] Bath gas, N_2; pressure, 1 atm; temperature range, 900−1300 K. [b] Units: cm^3, mol, s, cal.

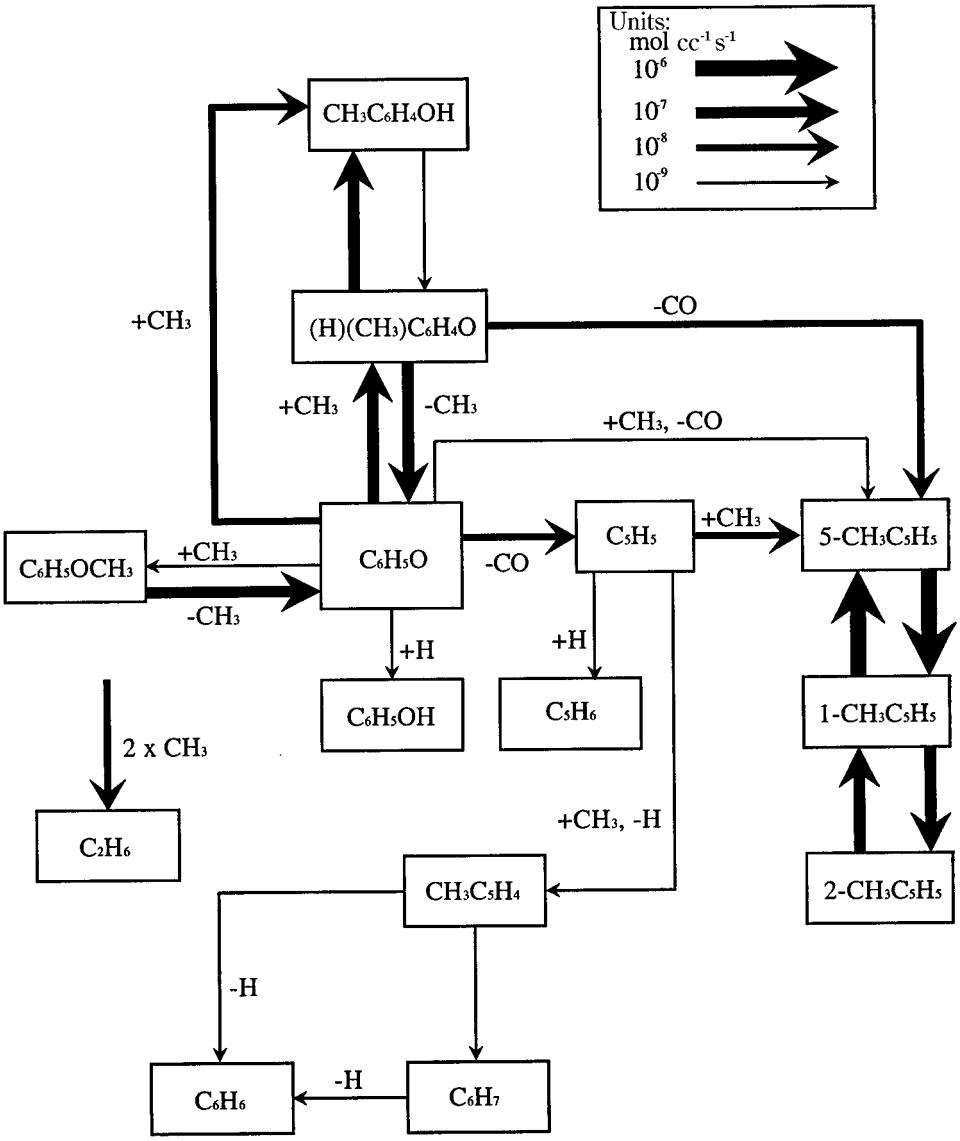

Figure 11. Flux at $t = 15$ ms.

TABLE 6: Activation Parameters[a] and Arrhenius Parameters[b,c] Calculated for [1,5] H Shifts of 5- and 1-$CH_3C_5H_5$

reaction	$\Delta H^{\ddagger}$	$\Delta S^{\ddagger}$	A	E_a	$k_{1000\ K}$
$5\text{-}CH_3C_5H_5 \rightarrow 1\text{-}CH_3C_5H_5$	33.1	−4.0	7.57E+12	35.1	1.62E+05
$1\text{-}CH_3C_5H_5 \rightarrow 2\text{-}CH_3C_5H_5$	53.7	3.0	2.56E+14	55.7	1.72E+02

[a] Calculated at the PM3 level of theory. [b] $E_a = \Delta H^{\ddagger} + RT$ and $A = (ekT/h)\exp(\Delta S^{\ddagger}/R)$. [c] Units: mol, s, kcal, K.

(assumed to have zero activation energy) was assigned $A = 5 \times 10^{13}$ cm^3 mol^{-1} s^{-1}. The activation energy for the reverse reaction, 97 kcal, is determined by thermodynamics. Clearly, this reaction cannot be a significant source of phenol at 1000 K. Modeling results support this conclusion. Attempts to model phenol via pathways involving recombination of phenoxy radicals and subsequent consumption of the dimers[43] were also unsuccessful.

Arends and co-workers[18] encountered a similar obstacle in predicting their observed phenol yields. In their anisole hydrogenolysis model, the rate of recombination of phenoxy and H to yield phenol had to be artificially increased (from the rate constant given above) by a factor of 50. Omission of this acceleration led to extreme overprediction of phenoxy concentration, accompanied by unrealistic yields of cresols. It was acknowledged by the authors, however, that a homogeneous bimolecular gas-phase reaction could not effect such a rapid rate. And, it was suggested that the conversion of phenoxy to phenol could have been accelerated by a heterogeneous process at the reactor wall as it is well-known that quartz reactors adsorb

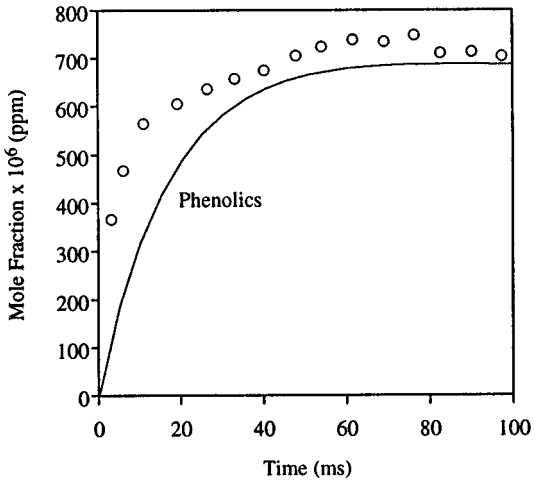

Figure 12. Comparison of experimental pyrolysis data and model prediction of total phenolics = C_6H_5OH + $CH_3C_6H_4OH$. Solid lines indicate model results.

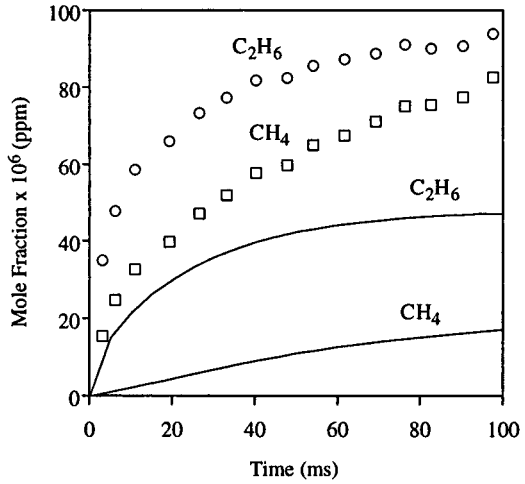

Figure 13. Comparison of experimental pyrolysis data and model prediction of methane and ethane. Solid lines indicate model results.

H atoms and catalyze recombinations. Similarly, Mackie and co-workers[17] found that significant fractions of both phenol and methane observed in their study could not be accounted for by homogeneous gas-phase recombination or abstraction reactions. The unaccounted for methane was shown to obey first-order kinetics, and the authors suggested the possible occurrence of surface-catalyzed chemistry.

Investigation of Surface Effects. The possibility of surface-mediated chemistry was investigated in the context of this modeling effort. It was found that model profiles could be corrected by the inclusion of pseudo-first-order rate constants for the wall-facilitated recombination of phenoxy and methyl with H of the order 10^3 s^{-1}. This value is well within the maximum allowable limit as calculated from kinetic theory[44] for the rate of wall collisions, $\sim 10^4$. Experimentally, however, no justification for the assumption of heterogeneous chemistry was found. A series of experiments was performed with the reactor test section replaced by another of one half the original diameter, increasing the surface to volume ratio by a factor of 2 and thus reducing the characteristic time of diffusion to the reactor wall by a factor of 4. It was postulated that condensed high molecular weight material on the test section surface might provide labile hydrogen for abstraction by gas-phase radicals. No change in the product distribution was observed in the initial trials. In an attempt to coat the quartz surface with a large amount of condensed material, anisole was then pyrolyzed in the reactor at an initial concentration several times that normally used. The experiments were repeated, and still no change in the chemistry was revealed. While this result represents a further validation of the Princeton flow reactor as a device capable of capturing homogeneous gas-phase chemistry, it leaves the mechanism of phenoxy conversion to phenol in the flow reactor as yet unresolved.

The difficulty in predicting successfully the fate of the phenoxy radical in intermediate- to high-temperature combustion experiments is pandemic. The anisole studies of Arends[18] and Mackie[17] are just two examples. Lindstedt and Skevis,[7] in their endeavor to model the benzene flame (where it is to be noted that no surface effect is possible) data of Bittner and Howard[45] and Hausmann et al.,[46] overpredicted phenoxy levels by a factor of 20. Zhang and McKinnon[8] attempted to model the same data overpredicting phenoxy concentration by 2 orders of magnitude. They noted that removal from their mechanism of the three primary phenoxy production channels still did not provide agreement with experiment and concluded that the error must lie in the phenoxy consumption channels.

Conclusions

Extensive experimentation revealed that the oxidation of anisole at atmospheric pressure near 1000 K did not differ significantly from its pyrolysis at the same nominal conditions. Reactions of phenoxy with methyl, loosely termed “pyrolytic”, to produce directly a number of the major species dominate the system chemistry even in the presence of oxygen.

The pyrolysis of anisole has been modeled with excellent agreement between experimental data and predictions of fuel decay and intermediates including methylcyclopentadiene, carbon monoxide, and total phenolics. Unmeasured rate constants were rigorously estimated, without adjustment to better fit the experimental data. The model’s primary shortcoming is its inability to predict correctly the relative distribution of phenol and cresols. The underprediction of methane and ethane is a symptom of this fault. Attempts to explain the discrepancy by the assumption of heterogeneous chemistry were successful within the context of modeling but were not validated experimentally. The resolution of this issue poses a challenging research problem and is expected to be aided by kinetic modeling of phenol oxidation data recently collected in this laboratory.

Acknowledgment. This work was supported by the Department of Energy, Office of Basic Energy Sciences, Division of Chemical Sciences, under Contract DE-FG02-86ER13554 and by the DoD/DOE/EPA Strategic Environmental Research and Development Program (SERDP).

References and Notes

(1) Mayotte, S. C.; Venkatesh, R.; Lindhjem, C. E.; Sklar, M. S. *SAE Trans.* **1994**, *103*, 1331.
(2) Westmoreland, P. R.; Dean, A. M.; Howard, J. B.; Longwell, J. P. *J. Phys. Chem.* **1989**, *93*, 8171.
(3) Frenklach, M.; Wang, H. American Chemical Society, National Meeting, Fuels Division, New York, 1991; p 1494.
(4) Nelson, P. F.; Quigley, S. M. *Atmos. Environ.* **1984**, *18*, 79.
(5) Bittker, D. A. *Combust. Sci. Technol.* **1991**, *79*, 49.
(6) Emdee, J. L.; Brezinsky, K.; Glassman, I. *J. Phys. Chem.* **1992**, *96*, 2151.
(7) Lindstedt, R. P.; Skevis, G. *Combust. Flame* **1994**, *99*, 551.
(8) Zhang, H.-Y.; McKinnon, J. T. *Combust. Sci. Technol.* **1995**, *107*, 261.
(9) Venkat, C.; Brezinsky, K.; Glassman, I. *Nineteenth Symposium (International) on Combustion*; The Combustion Institute: Pittsburgh, PA, 1982; p 143.
(10) Brezinsky, K. *Prog. Energy Combust. Sci.* **1986**, *12*, 1.
(11) Lin, C.-Y.; Lin, M. C. *Int. J. Chem. Kinet.* **1985**, *17*, 1025.
(12) Lin, C.-Y.; Lin, M. C. *J. Phys. Chem.* **1986**, *90*, 431.
(13) Olivella, S.; Solé, A.; García-Raso, A. *J. Phys. Chem.* **1995**, *99*, 10549.

(14) Frank, P.; Herzler, J.; Just, T.; Wahl, C. *Twenty-Fifth Symposium (International) on Combustion*; The Combustion Institute: Pittsburgh, PA, 1994; p 833.
(15) Paul, S.; Back, M. H. *Can. J. Chem.* **1975**, *53*, 3330.
(16) Suryan, M. M.; Kafafi, S. A.; Stein, S. E. *J. Am. Chem. Soc*. **1989**, *111*, 1423.
(17) Mackie, J. C.; Doolan, K. R.; Nelson, P. F. *J. Phys. Chem*. **1989**, *93*, 664.
(18) Arends, I. W. C. E.; Louw, R.; Mulder, P. *J. Phys. Chem*. **1993**, *97*, 7914.
(19) Brezinsky, K.; Litzinger, T. A.; Glassman, I. *Int. J. Chem. Kinet*. **1986**, *16*, 1053.
(20) Litzinger, T. A.; Brezinsky, K.; Glassman, I. *Combust. Flame* **1986**, *63*, 251.
(21) Emdee, J. L. An Experimental and Modeling Study of the High Temperature Oxidation of the Xylenes. Ph.D. Thesis, Department of Mechanical and Aerospace Engineering, Princeton University, Princeton, NJ, 1991.
(22) Sullivan, J. J. In *Modern Practice of Gas Chromatography*; Grob, R. L., Ed.; John Wiley & Sons: New York, 1977; Chapter 5.
(23) Supelco technical support staff, personal communication.
(24) Mulcahy, M. F. R.; Williams, D. J. *Aust. J. Chem*. **1965**, *18*, 20.
(25) Hart, H. *Chem. Rev*. **1979**, *79*, 515.
(26) Manion, J. A.; Louw, R. *J. Phys. Chem*. **1989**, *93*, 3563.
(27) Klinkenberg, W.; Louw, R. C. C. E. *Special Report Series*; Leiden University: Leiden, 1987; No. 87-01.
(28) Spielmann, R.; Cramers, C. A. *Chromatographia* **1972**, *5*, 295.
(29) Ritter, E. R.; Bozzelli, J. W.; Dean, A. M. *J. Phys. Chem*. **1990**, *94*, 2493.
(30) Kee, R. J.; Miller, J. A.; Jefferson, T. H. CHEMKIN: A General Purpose, Problem-Independent, Transportable, Fortran Chemical Kinetics Code Package. Sandia National Laboratory Report SAND80-8003, 1980.
(31) Kee, R. J.; Rupley, F. M.; Miller, J. A. The Chemkin Thermodynamic Data Base; Sandia National Laboratory Report SAND87-8215, 1987.
(32) Burcat, A.; McBride, B.; Rabinowitz, M. TAE Report No. 657, Technion, Haifa, 1990.
(33) Benson, S. W. *Thermochemical Kinetics*; John Wiley & Sons: New York, 1976.
(34) Ritter, E. R.; Bozzelli, J. W. THERM: Thermodynamic Property Estimation for Radicals and Molecules; computer code, New Jersey Institute of Technology, 1987.
(35) Cypres, R.; Bettens, B. *Tetrahedron* **1974**, *30*, 1253.
(36) Dean, A. M.; Bozzelli, J. W.; Ritter, E. R. *Combust. Sci. Technol*. **1991**, *80*, 63.
(37) Lin, C.-Y.; Lin, M. C. *Aust. J. Chem*. **1986**, *39*, 723.
(38) Spangler, C. W. *Chem. Rev*. **1976**, *76*, 187.
(39) McClean, S.; Haynes, P. *Tetrahedron* **1965**, *21*, 2313.
(40) Stewart, J. J. P. *J. Comput.-Aided Mol. Des*. **1989**, *4*, 1.
(41) He, Y. Z.; Mallard, W. G.; Tsang, W. *J. Phys. Chem*. **1988**, *92*, 2196.
(42) Kerr, J. A.; O'Grady, B. V.; Trotman-Dickenson, A. F. *J. Chem. Soc. A* **1967**, *6*, 897.
(43) Gopalan, S.; Savage, P. E. In *Innovations in Supercritical Fluids*; Hutchenson, K. W., Ed.; American Chemical Society: Washington, DC, 1995; Chapter 14.
(44) Somorjai, G. A. *Introduction to Surface Chemistry and Catalysis*; John Wiley & Sons: New York, 1972.
(45) Bittner, J. D.; Howard, J. B. *Eighteenth Symposium (International) on Combustion*; The Combustion Institute: Pittsburgh, PA, 1980; p 1105.
(46) Hausmann, M.; Hebgen, P.; Homann, K. H. *Twenty-Fourth Symposium (International) on Combustion*; The Combustion Institute: Pittsburgh, PA, 1992; p 793.
(47) Pitz, W. J.; Westbrook, C. K.; Proscia, W. M.; Dryer, F. *Twentieth Symposium (International) on Combustion*; The Combustion Institute: Pittsburgh, PA, 1980; p 831.
(48) Kerr, J. A.; Parsonage, M. J. *Evaluated Kinetic Data on Gas Phase Hydrogen Transfer Reactions of Methyl Radicals*; Butterworths: London, 1976.
(49) Dean, A. M. *J. Phys. Chem*. **1990**, *94*, 1436.
(50) Kopinke, F.-D.; Remmler, M.; Mensing, H.; Higo, P. *J. Phys. Chem*. **1994**, *98*, 1171.
(51) Ackermann, L.; Hippler, H.; Pagsberg, P.; Reihs, C.; Troe, J. *J. Phys. Chem*. **1990**, *94*, 5247.
(52) Kiefer, J. H.; Mizerka, L.; J.; Patel, M. R.; Wei, H.-C. *J. Phys. Chem*. **1985**, *89*, 2013.
(53) Fahr, A.; Stein, S. E. *J. Phys. Chem*. **1988**, *92*, 4951.
(54) Rao, V. S.; Skinner, G. B. *J. Phys. Chem*. **1989**, *93*, 1864.
(55) Bowman, C. T.; Hanson, R. K.; Davidson, D. F.; Gardiner, Jr., W. C.; Lissianski, V.; Smith, G. P.; Golden, D. M.; Frenklach, M.; Goldenberg, M. http://www.me.berkeley.edu/gri_mech/.
(56) Moreno, M.; Miller, W. H. *Chem. Phys. Lett*. **1990**, *171*, 475.
(57) Reid, R. C.; Prausnitz, J. M.; Poling, B. E. *Properties of Gases and Liquids*, 4th ed.; McGraw-Hill: New York, 1987.